Impact of Al-tobermorite formation on ion transport in cementitious materials

Abudushalamu Aili[a], Ippei Maruyama[a,b*], Yoshito Umeki[c], Kazuhiro Yokokura[d]

a: Graduate School of Environmental Studies, Nagoya University, Nagoya, Japan

b: Graduate School of Engineering, The University of Tokyo, Tokyo, Japan

c: Civil & Architectural Engineering, Department, Hamaoka Nuclear Power Station, Chubu Electric Power Company Incorporated, Shizuoka, Japan

d: Chubu Electric Power Co., Inc., Nuclear Safety Research & Development Center, Japan

* : corresponding author, i.maruyama@nagoya-u.jp

Abstract

In concrete structures intended for long-term use, the diffusion properties change over time with possible chemical reactions that may happen in the concrete. In this study, we performed a two-week Cesium Chloride diffusion test on cored samples from five different walls in a nuclear power plant. The reaction between feldspar group aggregates and cement paste was confirmed previously. We measured the diffusion profiles of Cesium and Chloride ions by electron probe micro analyzer. The diffusion of chloride ions was faster than cesium. Cesium was adsorbed into certain aggregates and replaced sodium, resulting in an anomalous diffusion profile. Taking into account the impact of charged surface of calcium aluminate silicate hydrates (C-A-S-H), we simulated the ionic diffusion with the finite difference method and obtained an apparent diffusion coefficient. The diffusion was slow in samples with lower calcium over alumina plus silica ratio of amorphous C-A-S-H. However, diffusion was more effortless in the samples containing the crystal form of C-A-S-H, Al-tobermorite. Such ease of diffusion could be attributed to the difference in morphology of C-A-S-H. In contrast to samples without Al-tobermorite, we observed higher cesium concentrations than chloride near the diffusion surface in samples with Al-tobermorite. It seems that the cesium was adsorbed in cement paste by exchanging with alkali on Al-sites.

Keywords: Ionic diffusion, tortuosity, Al-tobermorite, aged concrete, cesium adsorption

Article Highlights

- Cesium chloride diffusion tests were performed on saturated samples of aged

concrete containing Al-tobermorite/no Al-tobermorite.

- The apparent diffusion coefficient was lower for the samples with lower Ca/(Al+Si) in the amorphous phase of cement paste.
- Samples containing Al-tobermorite showed lower tortuosity and higher uptake of cesium.

1 Introduction

The transport of ions in cement-based materials has been widely studied since it is one of the most common phenomena for any concrete structure whose surfaces are not perfectly coated. Invasion of ions from the surrounding environment to the concrete is susceptible to degrading the concrete's properties and reducing the structure's service life. Such degradation includes chloride-induced corrosion of reinforcing steel bars, carbonation, and alkali-silica reactions. The invading ions first penetrate the surface of the concrete and then transport further into the internal part via the pore network by diffusion, migration, advection, and capillary suction. In saturated concrete, which is the case of the inner part of thick concrete structures, diffusion through pores is the predominant mechanism.

Diffusion of the ions depends on environmental factors and the material properties, especially the microstructure and phase composition of cement paste. In Portland cement paste, the calcium silicate hydrates (C-S-H) are the main phase accounting for more than 60% of the volume. C-S-H is composed of a central calcium oxide layer, on which silica is attached in the form of dimers. When the pairing silica dimers are not connected, the general case known as empty bridging positions, interlayer calcium ions will be more concentrated in some places, causing more water. As a result, the main calcium layers are winded, forming larger and smaller spaces (Gartner et al. 2017). These larger spaces are called gel pores, while the smaller spaces are known as interlayer spaces. The network of gel pores and interlayer spaces, together with the high specific surface area, makes the C-S-H the main diffusion media for invading ions. At the interface with water in gel pores and interlayer space, the silanol group deprotonates (i.e., loses an H^+), which is then compensated by calcium ions resulting in a positively charged surface (Lothenbach and Nonat 2015; Richardson 2014). These positively charged surfaces of C-S-H accelerate the diffusion of anions while decelerating that of cations (Goto and Roy 1981; Johannesson et al. 2007). Furthermore, the chloride ions can be physically adsorbed on C-S-H, reducing the rate of diffusion (Martín-Pérez et al. 2000).

Chloride ions are also bounded chemically to other hydrates such as monosulfoaluminate (AFm) (Georget et al. 2022a) and Friedel's salts (Shi et al. 2017).

Concerning the analysis and modeling of diffusion, Fick's law was applied in the beginning (Maage et al. 1996; Page et al. 1981; Thomas and Bamforth 1999). Later, improved models were developed by considering the interaction between the solid phase and ions. Specifically for chloride ions, for instance, (Martín-Pérez et al. 2000; Xi and Bazant 1999) considered the physical or chemical adsorption in the modeling. The importance of the electrical double layer that formed near the surface of C-S-H was pointed out (Elakneswaran et al. 2009; Goto and Roy 1981) and considered in (Elakneswaran et al. 2010; Friedmann et al. 2008; Samson et al. 2000). Since the interaction between various ion species that are diffusing cannot be treated independently (Gupta et al. 2019), multi-ionic diffusion models were proposed (Johannesson et al. 2007; Samson et al. 2000) and further developed (Hosokawa et al. 2011; Kari et al. 2013; Samson and Marchand 2007). Recently, (Ichikawa 2022) pointed out several shortcomings of many models, such as insufficient consideration of electrical neutrality conditions. In the same work, (Ichikawa 2022) constructed a new model for ion diffusion in porous solid with surface charge, departing only from three fundamental laws: the general theory of diffusion, Gauss's law, and electrical neutrality condition. However, complex models require sophisticated material parameters as input, compromising the applicability and accuracy of prediction. To assess the durability of concrete structures in the long term, (Sui et al. 2019) proposed a more generic approach based on multiple experimental techniques, while (Georget et al. 2022b) discussed the merit of using Fick's law, which is the origin of the so-called square-root law.

Most of the studies were performed on laboratory-made cement paste and concrete samples. In engineering practice, the properties of aged concrete could be somewhat different from that of laboratory-made ones after long-term use. For instance, in massive concrete walls of the decommissioning Hamaoka nuclear powerplant, the cement hydrates reacted with the silica and alumina released from feldspar group aggregates after 16½ years of operation under a relative humidity higher than 80% (Rymeš et al. 2019). As a result, alumina was incorporated into C-S-H. It formed calcium aluminate silicate hydrates (C-A-S-H), whose calcium over silica (Ca/Si) molar ratio decreased (Maruyama et al. 2021). In the walls whose temperature during the operation was higher than ~40 °C, crystal form of C-A-S-H, Al-tobermorite was formed. Such changes, i.e. changes in tortuosity of pores, reduction of microstructural surface, and surface charge of hydrates affect the transport of ions. Taking the alkali ions (such as sodium or

potassium) which diffuse together with chloride ions, the alkali binding in C-S-H/C-A-S-H increases with the decrease of the Ca/Si molar ratio (Johannesson et al. 2007) and also with the presence of alumina (Hong and Glasser 2002). Experimental studies on such aged concrete are necessary to understand the in-situ condition better and deal with accidents such as the contamination of concrete structures by radionuclides in the Fukushima accident (Tomita et al. 2021). And the obtained data also give an inspiration how the elements diffuse in the system after formation of Al-tobermorite in the system of a nuclear geological disposal (Dauzeres et al. 2010; Martin 1994). We performed hence cesium chloride diffusion experiment using cored concrete specimens from the walls mentioned above of the Hamaoka nuclear powerplant, aiming to shed some light on the impact of Al-tobermorite formation on diffusion properties of concrete. Since the concrete samples do not contain cesium, cesium was preferred instead of sodium or potassium. The diffusion profiles were measured by an electron probe micro analyzer (EPMA), which was proven to be an efficient method in evaluating the diffusion profiles (Elakneswaran et al. 2010; Mori et al. 2006) .

2 Material and method

2.1 Sample

The samples were from unit 1 of the Hamaoka Nuclear Power Plant located in Omaezaki, Shizuoka Prefecture, Japan. Two samples were from internal wall #1 (IW1), and three were from the biological shielding wall (BSW). The mixture proportions of the concrete of the two walls are given in Table 1.

Table 1 Mixture proportion of the concretes (Horiuchi et al. 1975)

	Design Strength	Cement type*	Slump (cm)	Air (%)	Maximum aggregate size (mm)	Water to cement ratio	Sand volume to aggregate volume ratio	Cement	Water	Sand	Gravel (5–25 mm)	Water reducing agent**(mass % per cement)
								(kg/m^3-concrete)				
IW1	22.1	O	12	3.5	25	48.3	38.5	300	145	734	1178	0.750

BSW	22.1	M	12	3.5	25	48.0	39.7	300	144	758	1160	0.750

*Cement type: O: ordinary Portland cement; M: moderate-heat Portland cement (according to the Japanese Industrial Standard JIS R 5210(JSA 1973)).

**Water reducing agent: lignin-based water reducing agent.

Cylindrical samples with a height of 5 cm and diameter of 10 cm were cored from different locations of the walls with air-cooled dry coring to avoid any loss of ions (such as washing away calcium ions). Samples were denoted with the wall's name followed by the distance between the core center and the wall's surface: IW1-100, IW1-500, BSW-100, BSW-100, BSW-380, and BSW-1085. Maruyama et al., (Maruyama et al. 2021) reported the mineral composition of these samples from quantitative XRD Rietveld analysis and confirmed that feldspar group aggregates dissolved and reacted with cement hydrates. Al-tobermorite was present in BSW-380 and BSW-1085 but not in IW1-100, IW1-500, and BSW-100. Concerning the diffusion of cesium and chloride ions, we retrieved the following information from (Maruyama et al. 2021)Table 2: monosulfoaluminate (AFm), Al-tobermorite content of the samples, and the reaction degree of aggregates (summarized in Table 2). The reaction degree of aggregate was defined as the mass ratio of the aggregates that reacted with cement hydrates over the total amount of aggregates in the initial mixture.

Table 2 AFm, Hydrogarnet, Al-tobermorite content, and reaction degree of the aggregate of the samples (data are from (Maruyama et al. 2021))

Sample	AFm per cement paste [%]	Al-tobermorite per cement paste [%]	Reaction degree of aggregate [%]
IW1-100	0.67	0.00	2.65
IW1-500	0.20	0.00	2.53
BSW-100	0.09	0.00	3.69
BSW-380	0.00	12.46	6.20
BSW-1085	0.00	4.37	5.88

From the cylindrical sample of 5 cm height and 10 cm diameter, we cut a prism sample

of section 15 mm × 25 mm and height of 5 cm and immersed the sample into saturated lime water, stored at 20 °C for 28 days. Then, for each specimen, one surface of 15 mm × 25 mm was designated as the surface of diffusion, and all other fives surfaces were coated with epoxy (Infraguard CRJ S, Sekisui chemical co.,) which is impermeable against water.

2.2 Experiment

After the epoxy hardening, samples were immersed in a cesium chloride solution of concentration 0.5 M. One-dimensional diffusion under such conditions continued for 15 days.

At the end of the diffusion test, we cut samples along a perpendicular direction to the diffusion surface with a Diamond saw using oil as a lubricant to avoid any perturbance on the diffusion profile of cesium and chloride ions. Lubricant oil was also used during the subsequent polishing of the sample surface. The oil was washed away by ultrasonic washing in isopropanol. Then, the samples were dried and kept under a vacuum for five days before being sealed and kept for observation under an electron probe micro analyzer (EPMA).

The surface of the samples was mirror polished and coated with carbon to enhance the conductivity. Elemental distributions on the surfaces were measured using a JXA-8100 (JEOL Ltd., Japan). Measurement settings were as follows: accelerator voltage: 15 kV, probe current: 200 nA, probe diameter: 50 µm, spatial resolution (i.e., pixel size): 100 µm × 50 µm, measurement interval: 40 ms/pixel. The elements measured in EPMA were Cs, Cl, Na, K, CaO, Si, Al, S, Fe, and Mg. Measurement results were expressed in mass fraction of elements (Cs and Cl) or oxides (Na_2O, K_2O, CaO, SiO_2, Al_2O_3, SO_3, Fe_2O_3, and MgO).

3 Experimental results

The cesium and chloride ion distributions from EPMA scanning are shown in Figure 1. Combining with the optical photograph of the samples and distribution maps of other elements (specifically CaO, SiO_2, Al_2O_3), we can distinguish cement paste from aggregates and see that chloride ions diffused only through cement paste. As for cesium ions, we can observe adsorption by some aggregates in addition to the diffusion mainly through cement paste.

To obtain the diffusion profiles of cesium and chloride ions in the cement paste, we

removed the pixels belonging to aggregates following the method presented by (Mori et al. 2006). The criteria of cement paste are expressed in the average value of 18 mm width (central part in the 25 mm of sample width) as follows: CaO < 10 mass%, 12 mass% < SiO_2 < 35 mass% (for IW1-100 and BSW-100) or 20 mass% < SiO_2 < 45 mass% (for all the other samples). The obtained distribution maps of cesium and chloride ions on cement paste are displayed in Figure 1.

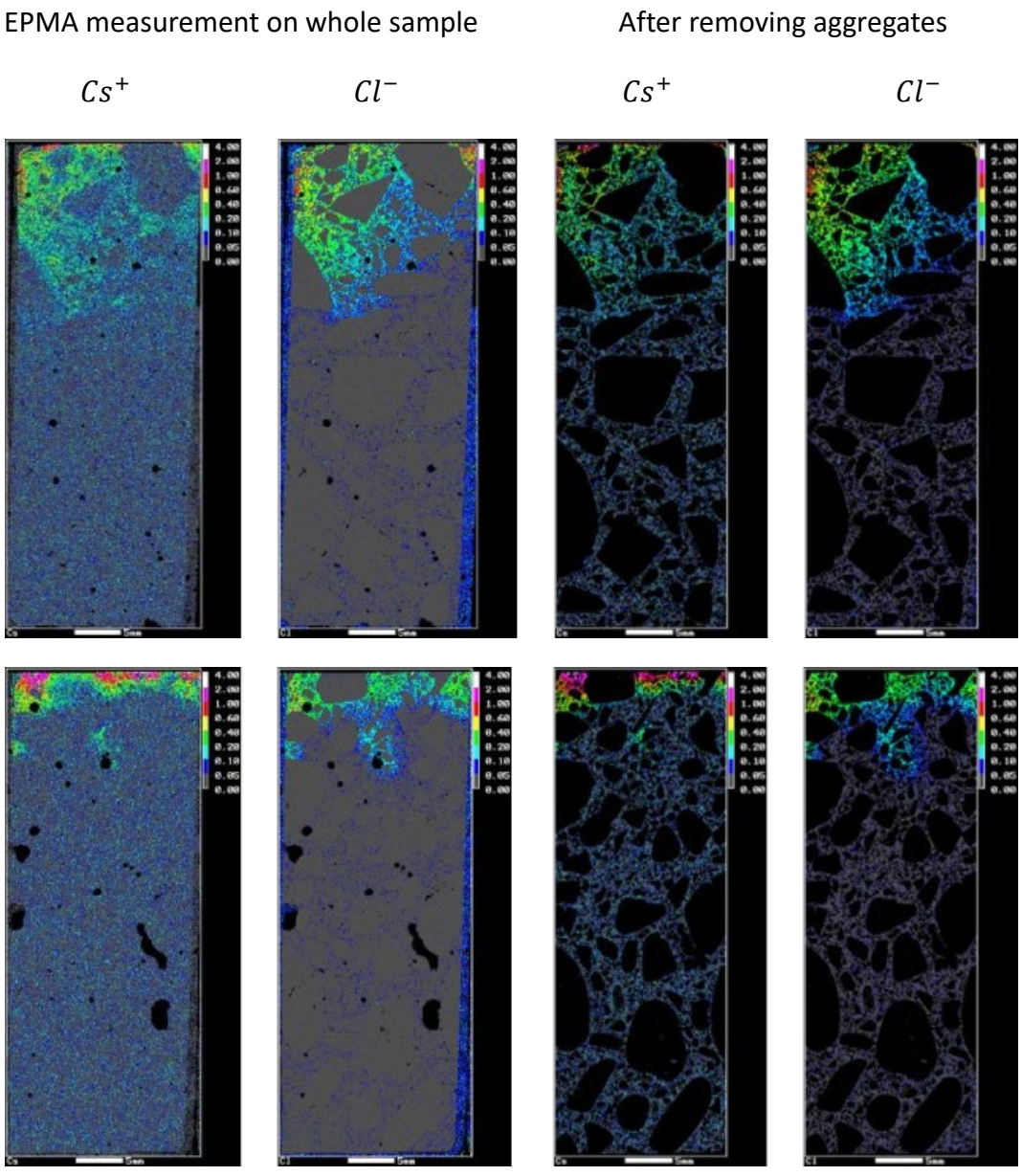

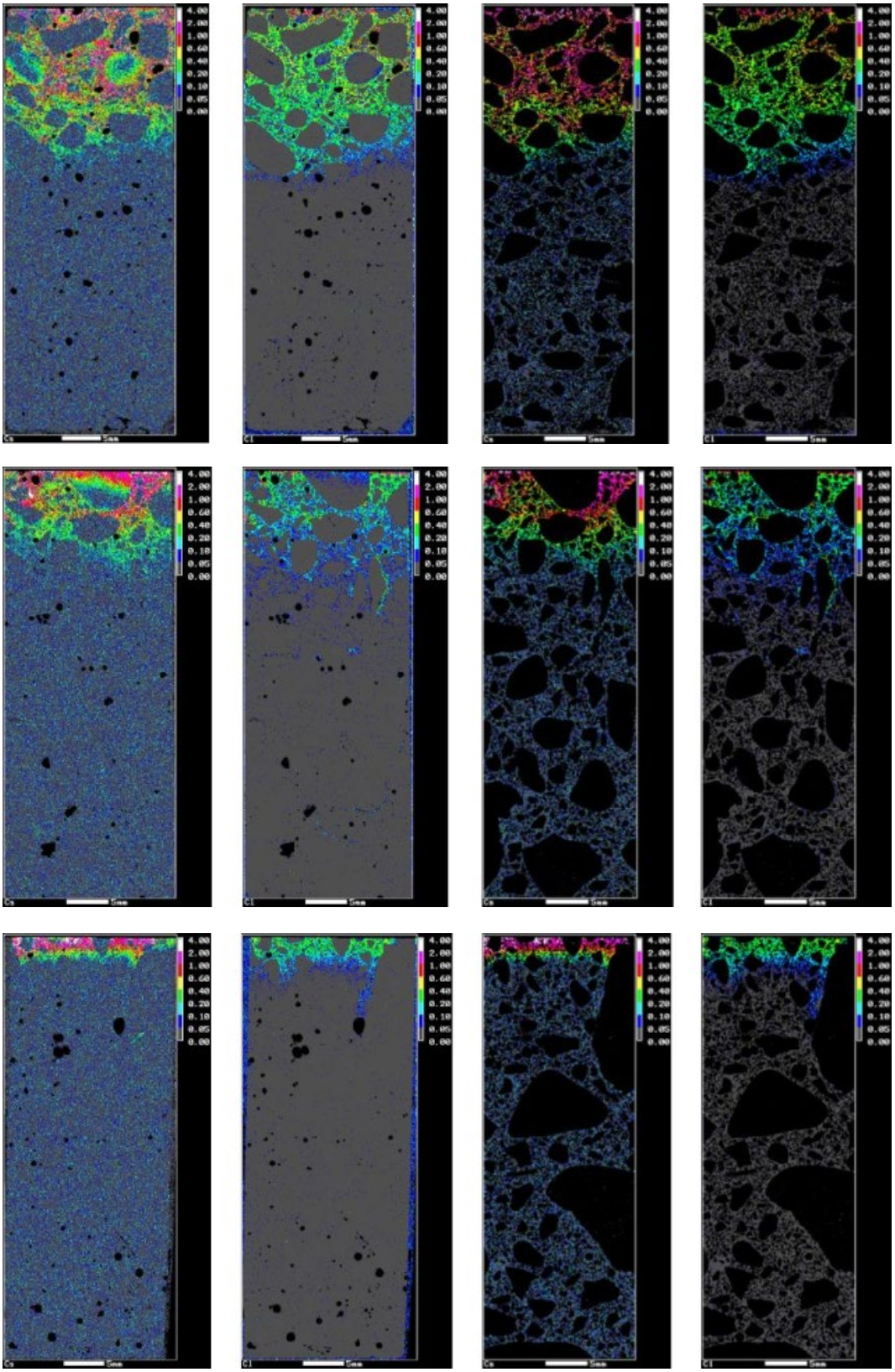

179 Figure 1 Distribution maps of cesium and chloride ions obtained from EPMA scanning.

From top row to bottom: IW1-100, IW1-500, BSW-100, BSW-380, BSW-1085.

Integrating the distribution maps on cement paste along the width, we obtained the diffusion profile of cesium and chloride as a function of the diffusion distance. The diffusion profiles are shown in Figure 2. For all the specimens, the diffusion of chloride ions was faster than that of cesium ions. Chloride molar concentration was higher than cesium all along the diffusion profile, except for the near-surface parts in the specimens BSW-380 and BSW-1085. In the sample BSW-100, a local minimum was observable around the diffusion distance of 4 mm for both cesium and chloride. We assume that this abnormality is caused by aggregate and discuss the role of aggregate in section 5.34. As the article's main objective is diffusion through cement paste, we will analyze the diffusion profiles and estimate the diffusion coefficient in the next section.

4 Estimation of the diffusion coefficient

Fick's law is the most straightforward way to analyze the diffusion rate from the concentration profiles in Figure 2. Though Fick's law oversimplifies the diffusion through C-A-S-H, it has been shown by (Georget et al. 2022b) that it is still applicable when other phenomena, such as binding, are at equilibrium (i.e., not time-dependent). Since the cesium and chloride ions diffuse through the pores of C-A-S-H and interact with the charged surfaces, we acknowledge the importance of considering such charged surfaces' role. Therefore, in the following, we estimate the diffusion rate of cesium and chloride by using Fick's law and then by a model that accounts for the impact of charged surface on the ionic diffusion.

4.1 Fick's law

Fick's law states that the gradient of concentration drives diffusion. Noting the flow and concentration of ion i ($i = Cs^+, Cl^-$) as j_i and C_i, respectively, Fick's law reads as:

$$j_i = -D_i \nabla C_i, \tag{1}$$

With Di, the diffusion coefficient of ion i. In the case of one-dimensional diffusion, like in the experiment of this study, inserting the above Fick's law Eq.(1) into the following transport equation,

$$\frac{\partial C_i}{\partial t} = -\frac{\partial j_i}{\partial x}, \tag{2}$$

with x being the distance from the sample surface and t being the diffusion time, we

obtain the standard diffusion equation:

$$\frac{\partial C_i}{\partial t} = D_i \frac{\partial^2 C_i}{\partial x^2}, \quad (3)$$

The analytical solution of the above Eq.(3) gives us the diffusion profile of ion i at time t:

$$C_i(x,t) = C_i^0 \left(1 - erf\left(\frac{x}{2\sqrt{D_i t}}\right)\right) + C_i^\infty. \quad (4)$$

Since the concentration profile is a function of $x/\sqrt{t}$, Fick's law-based diffusion solution is also known as square-root diffusion. In the case of the experiment, before diffusion, the initial concentrations of cesium and chloride in the samples were zero, which translates as $C_i^\infty = 0$.

Fitting the measured diffusion profiles in Figure 2 to Eq.(4), we obtained diffusion coefficients for cesium and chloride in each sample. It should be noted that, while fitting Eq.(4) to the measured ion concentration profiles, we neglected the measurement of the first 1 mm depth considering possible calcium leaching. Furthermore, we neglected the irregularities caused by aggregates, such as the local minimum near the surface in IW1-500, BSW-100, faster decrease, and the shoulder towards the diffusion front in IW1-100 and IW1-500, respectively. The results are displayed in Figure 2, marked as Fick's law.

The above fitting gave an apparent diffusion coefficient D_i and an ionic concentration C_i^0 on the surface. The following section will use these concentrations on the surface as boundary conditions, which was the other motivation for using Fick's law in this study.

4.2 Ionic diffusion in porous solid with surface charge

To consider the impact of the charged surface of C-A-S-H solid layers on ionic diffusion, we referred to the theory of ionic diffusion in water-saturated porous solid with surface charge developed (Ichikawa 2022). We assume that the solid surface along the diffusion path is positively charged with a density of E, and that the positive charge is equilibrated with movable OH^- anions of concentration $C_{OH^-}^{ic}$, which will be exchanged with the diffusing Cl^-. Hence, this section considers three types of ions, i.e., $i = Cs^+, Cl^-, OH^-$.

The general theory of diffusion states that the driving force of diffusion is the gradient of chemical potential μ (Ichikawa 2022). Assuming that the chemical potential μ_i of

ion i is composed of free energy of dilution and electrostatic energy, for the monovalent ions, the chemical potential reads as:

$$\mu_i = RTlnC_i + z_iFU, \tag{5}$$

R and T are the universal gas constant and temperature; F and U are the Faraday constant and molar electrostatic potential. z_i is the charge valence, i.e., equals +1 for Cs^+, and -1 for Cl^-, OH^-. Thus, we obtained the flow of the ion according to the general theory of diffusion as follows:

$$j_i = -D_i\left(\nabla C_i + \frac{z_iFC_i}{RT}\nabla U\right). \tag{6}$$

In the case of one-dimensional diffusion, like in the experiment of this study, inserting the above Eq.(6) to the transport Eq.(2), we obtain:

$$\frac{\partial C_i}{\partial t} = D_i\frac{\partial^2 C_i}{\partial x^2} + D_i\frac{\partial}{\partial x}\left(z_iC_i\frac{F}{RT}\frac{\partial U}{\partial x}\right) \tag{7}$$

The electrostatic potential in the above equation can be obtained by considering the condition that the diffusion of ions does not generate an electrical current, which reads as:

$$j_{Cs} = j_{Cl} + j_{OH}. \tag{8}$$

Inserting the flow ions of Eq.(6) into the above Eq.(8), we obtain the electrostatic potential as:

$$\frac{F}{RT}\frac{\partial U}{\partial x} = \frac{D_{OH}\frac{\partial C_{OH}}{\partial x} + D_{Cl}\frac{\partial C_{Cl}}{\partial x} - D_{Cs}\frac{\partial C_{Cs}}{\partial x}}{D_{Cs}C_{Cs} + D_{Cl}C_{Cl} + D_{OH}C_{OH}} = \Theta(D_i, C_i). \tag{9}$$

Finally, by replacing the electrostatic potential in Eq.(7) with Θ of Eq(9), we obtain the partial differential equation system that governs the diffusion in the sample:

$$\frac{\partial C_i}{\partial t} = D_i\frac{\partial^2 C_i}{\partial x^2} + z_iD_i\left(\Theta\frac{\partial C_i}{\partial x} + C_i\frac{\partial \Theta}{\partial x}\right). \tag{10}$$

In contrast to Fick's law, in Eq.(10)(3), the diffusion of cesium and chloride ions are coupled with each other in the above Eq.(3)(10). The solution of Eq.(10) requires us to specify the boundary and initial conditions.

The boundary conditions include the concentration of ions at the sample surface $x = 0$ for any time t. In the outer solution, the OH- concentration is too low compared with Cs^+ and Cl^-concentrations. We take $C_{OH^-}^{bc}$ of OH^- at the sample surface equal to zero. Considering the irregularities on the sample surface in the measured diffusion profiles, we take the concentrations $C_{Cs^+}^{bc}$ and $C_{Cl^-}^{bc}$ of Cs^+ and Cl^- at the sample surface from the fitting results C_i^0 of section 4.1, not from the measurement.

The initial conditions include the concentrations of ions along the whole diffusion path at time $t = 0$. The initial Cs^+ and Cl^- concentrations are equal to zero. The concentration $C_{OH^-}^{ic}$ of OH^- should be equal to the surface charge density E. However, without direct measurement and a simple estimation method, *we considered* $C_{OH^-}^{ic}$ as a fitting parameter.

Given that the governing Eq.(10) is coupled with high-order partial differential equations, we used the finite difference method with the Forward Euler scheme. We constrained step length Δt and mesh size Δx that satisfy $D_i \Delta t / \Delta x^2 = 0.2$ to assure the convergence. Further, we assumed that the self-diffusion coefficient of OH^- and Cl^- are the same, $D_{OH^-} = D_{Cl^-}$, to reduce the number of fitting parameters. Then, adjusting the two diffusion coefficients D_{Cs^+} and D_{Cl^-}, and the initial concentration $C_{OH^-}^{ic}$ of the movable OH^- ions, a quasi-best fit to the experimental measurement was obtained and compared with the experimental results in Figure 2.

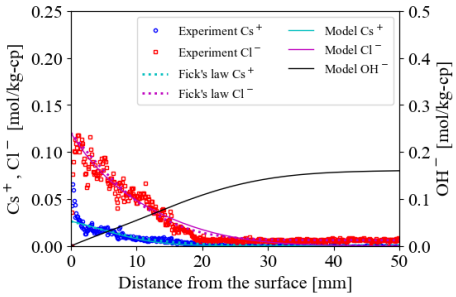

(a) IW1-100

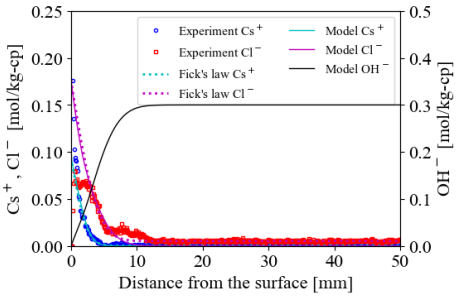

(b) IW1-500

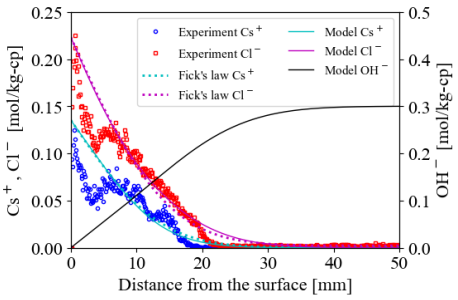

(c) BSW-100

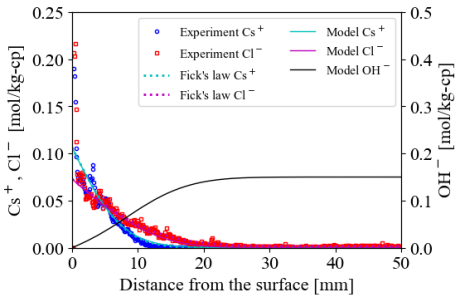

(d) BSW-380

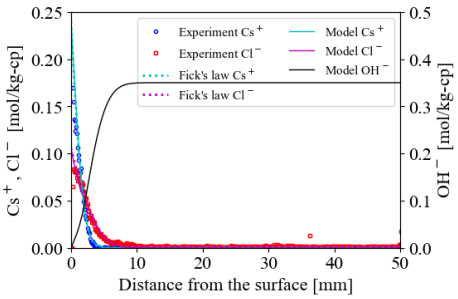

(e) BSW-1085

Figure 2 Diffusion profile of cesium and chloride ions along the height of the specimens. Points are experimental results from EPMA maps; Dashed lines are fittings with Fick's law Eq.(4); Continuous lines are fittings of ion diffusion model with surface charge, Eq.(10).

The apparent diffusion coefficients from the ionic diffusion model are compared with the apparent diffusion coefficient obtained from Fick's law in Figure 3. Since there is no significant difference between the apparent diffusion coefficients obtained from the model and Fick's law, we will use the apparent diffusion coefficient obtained from the model in the following.

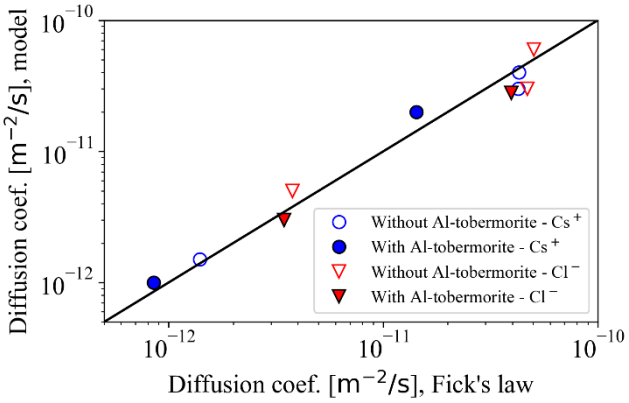

281

282 Figure 3 Comparison of the apparent diffusion coefficients obtained from the ionic
283 diffusion model with those from Fick's law.

284 5 Discussion

285 5.1 Impact of Al-tobermorite on diffusion properties

286 A helpful indicator for engineering applications is penetration depth. In this study, we
287 define the depth at which the concentration of ions is equal to 5% of the ion
288 concentration on the sample's surface. Considering that the presence of aggregate
289 perturbates the experimental diffusion profiles, we computed the penetration depth
290 from the computed diffusion profile of the model in section 4.2.

291 Another indicator to characterize the difficulty of diffusion is tortuosity (Garboczi 1990),
292 defined as the square root of the ratio between self-diffusion coefficient D_i^{self} and the
293 experimental diffusion coefficient D_i,

$$\lambda_i = \sqrt{\frac{D_i^{self}}{D_i}}. \tag{11}$$

294 Taking the self-diffusion coefficients as 1.95×10^{-9} m^2/s for both cesium and chloride (CSJ
295 2004), we computed the tortuosity of each sample for both ions.

296 In the concrete samples, the ions diffuse mainly through the pore network of the cement
297 paste. The total porosity of these samples was very similar, differing from each other by
298 less than 0.015 cm^3/cm^3. We assume hence that the difference in the diffusion
299 properties is caused not by the pore volume but mainly by the difference in the
300 connectivity of pores and surface charge difference. Such differences were due to the
301 environmental condition these samples were exposed to during the 16.5-year service

time. The penetration depth of cesium and chloride ions are plotted in function of the distance between the core center and the wall surface in Figure 4a and compared with the penetration depth measured in a similar diffusion test on ordinary Portland cement paste with the water-to-cement ratio of 0.6 (Ichikawa et al. 2021). The penetration depths of both cesium and chloride ions are smaller for samples from the inner part of the walls, where took place more reaction between feldspars and cement hydrates to form C-A-S-H and other phases. After 16.5 years of usage, inner parts of the concrete wall show a smaller penetration depth than a well-cured laboratory specimen. Figure 4b displays the penetration depths of both cesium and chloride ions in the function of the relative humidity of the core, measured at the time of coring on cores obtained by an air-cooling dry coring technique. The higher the core's relative humidity at the coring time, the less deep the ions penetrate in the sample.

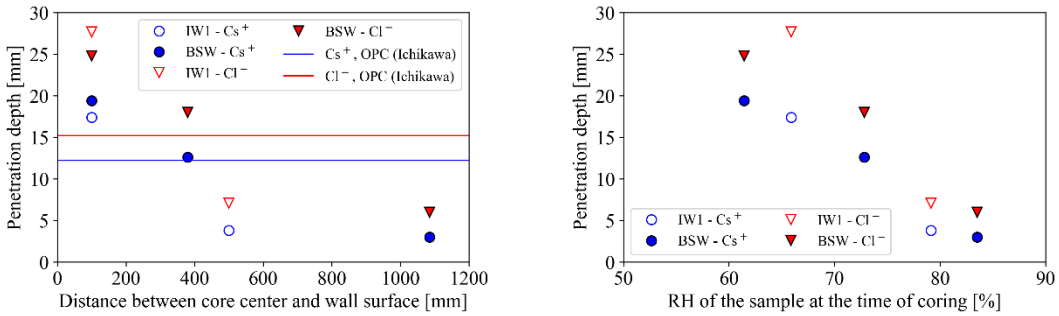

(a) (b)

Figure 4 Penetration depth of the ions in the function of (a) core position; (b) relative humidity of the core at the coring.

Given the similar porosity of the samples, the chemical composition and morphology of the hydrates are the main factors influencing the diffusion properties. The main hydrate phase C-A-S-H in these cores differ due to the reaction between the cement paste and feldspar group aggregates. The chemical composition and morphology of C-A-S-H are characterized by molar ratios between Ca, Si, and Al. We plot hence in Figure 5, the penetration depths in the function of Ca/(Al+Si) molar ratio of amorphous C-A-S-H, which were reported in (Maruyama et al. 2021) from measurements of energy dissipative X-ray spectroscopy (EDS).

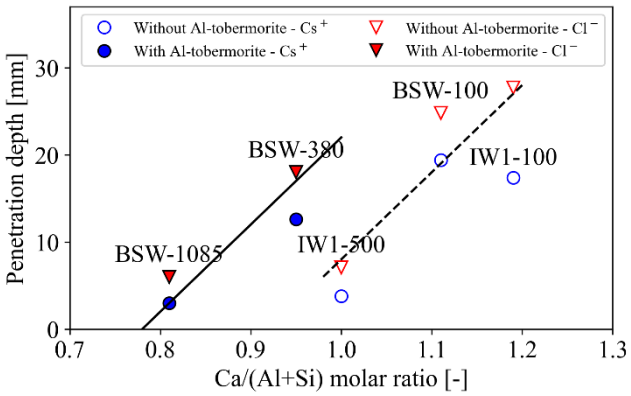

Figure 5 Penetration depth of Cs^+ and Cl^- in the function of Ca/(Al+Si) molar ratio of the amorphous C-A-S-H

Similarly, the tortuosity calculated using Eq.(11) is displayed in the function of the Ca/(Al+Si) molar ratio of the amorphous C-A-S-H in Figure 6. The results in Figure 5 and Figure 6 indicate that, with the decrease of calcium in amorphous C-A-S-H, the penetration depth decreased, and the tortuosity increased. In other words, diffusion becomes difficult when the amorphous C-A-S-H includes more silica and alumina. Nevertheless, when the Ca/(Al+Si) ratio is lower than 1, which is the case for the samples containing Al-tobermorite, the diffusion becomes easier (i.e., smaller tortuosity and larger penetration depth). It is stated in (Richardson 2004) that the morphology of C-S-H changes from fibrillar to foil-like when the Ca/Si ratio decreases. It is possible to suppose that the morphology of C-A-S-H in the samples containing Al-tobermorite differs significantly from that in the samples containing no Al-tobermorite. FFigure 5 and Figure 6 show that the critical Ca/(Al+Si) at which the morphology of C-A-S-H changes from fibrillar to foil-like might be around 1. We attribute the ease of diffusion in the samples containing Al-tobermorite to the difference in morphology of C-A-S-H.

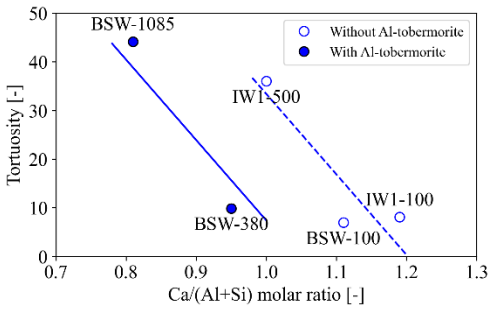

(a) Cs^+

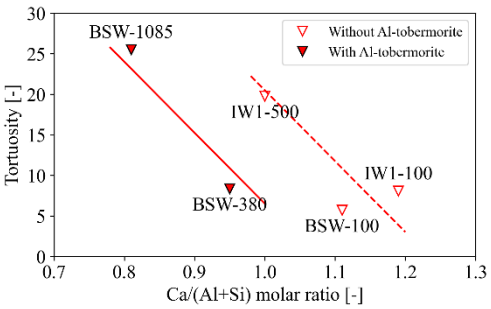

(b) Cl^-

Figure 6 Tortuosity in the function of Ca/(Al+Si) of amorphous C-A-S-H.

5.2 Adsorption of cesium in cement paste

Due to the ion exchange between OH^- and Cl^-, the chloride concentration is generally higher than cesium. However, in the measured diffusion profiles, the cesium concentration was higher near the surface in BSW-380 and BSW-1085. The shape of diffusion profiles in these two samples confirms this higher cesium concentration. Hence this is not caused by the irregularities near the surface. We assume that cesium ions were adsorbed on the cement paste. To compare the ability of cesium adsorption, we plotted the cesium concentration on the surface as a function of the molar ratio Ca/(Al+Si) in Figure 7a. Cesium adsorption is preferred for a lower Ca/(Al+Si) ratio, like other alkali ions such as sodium and potassium.

The aluminum in amorphous C-A-S-H is considered to be able to adsorb alkali ions (Hong and Glasser 2002). However, aluminum's role is difficult to confirm when cesium concentration on the sample surface is plotted as a function of the Al/(Al+Si) ratio. Na and K have probably already been adsorbed on the Al-site in C-A-S-H, and only exchange between Cs and Na, K can happen on the Al-sites during the diffusion test. To check the such hypothesis, we roughly estimated the molar ratio (Na+K)/Al in C-A-S-H. The method is as follows: combining the Inductively coupled plasma atomic emission spectroscopy measurement data and Rietveld analysis results of (Maruyama et al. 2021), we computed the alumina amount in each hydrate phase. We then took the average value of Al_2O_3 along the sample height from EPMA measurement as the total alumina and computed its portion in each hydrate. Comparing the obtained amount of alumina in C-A-S-H with Na_2O and K_2O from EPMA measurement, we estimated (Na+K)/Al molar ratio in C-A-S-H. Figure 7(b) displays the concentration of cesium on the sample surface in the function of the (Na+K)/Al molar ratio. Though scattered, the results show that a higher alkali content per alumina corresponds to a higher cesium concentration on the sample surface.

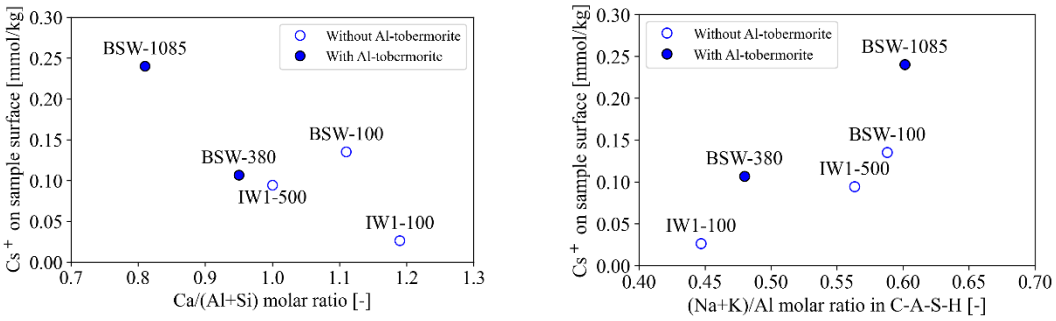

(a) (b)

Figure 7 Concentration of Cs^+ on the surface (a) as function of molar ratio Ca/(Al+Si); (b) as function of Al/(Al+Si).

5.3 Adsorption of cesium by aggregates

This section discusses the adsorption of cesium by the aggregates. The original EPMA maps of cesium distribution in Figure 1 show that cesium is adsorbed in certain aggregates of samples IW1-500, BSW-100, and BSW-380. The penetration depth of cesium and the sizes of aggregates make the sample BSW-100 best to observe cesium adsorption by the aggregates. We marked the contour of five aggregates near the surface of BSW-100 with color and numbered them on the optical photograph in Figure 8a. The EPMA maps of cesium, Na_2O, K_2O, SiO_2, and Al_2O_3 are shown in Figure 8b-f.

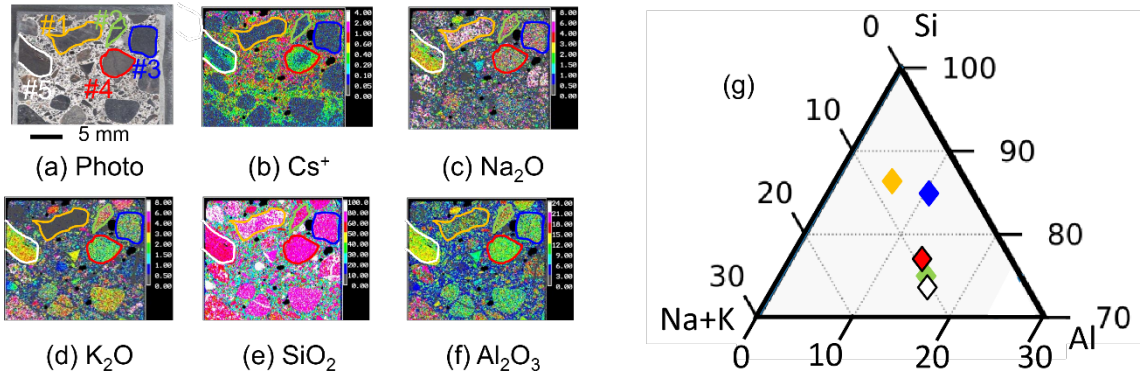

Figure 8 Cesium adsorption on aggregate in BSW-100: (a)-(f) photo, cesium and elemental composition of five aggregates; (g) ternary diagram (in molar ratio) showing the chemical composition of the five aggregates. Aggregate numbering-contour color: #1-orange, #2-green, #3-blue, #4-red, #5-white. The color of diamonds in (g) corresponds to the color of aggregate contour in (a).

Two of the five aggregates adsorbed cesium: i.e., #4 and #5. In aggregate #4, cesium

concentration reduced gradually from the contour of aggregate towards the center. In aggregate #5, cesium leached into from the left upper corner of the aggregate, while it can be seen that sodium leached out from the same position. It is possible to consider that in aggregate #5, cesium replaced sodium. Based on the EPMA maps, we estimated the chemical compositions of these aggregates and plotted them in a ternary diagram of silica, alumina, and alkali in Figure 8g. Higher alumina content is necessary for the aggregate to adsorb cesium. However, the chemical composition is insufficient for aggregates to adsorb cesium. Aggregate #2 has a similar composition as aggregates #4 and #5 but did not adsorb cesium. The density of the aggregate, which can be roughly distinguished from the darkness of color in the photograph Figure 8a, may also play a role in the cesium adsorption.

6 Conclusion

One-dimensional diffusion tests were performed for two weeks on concrete samples cored from the walls of a decommissioning nuclear power plant. Some samples contained Al-tobermorite while others did not. The diffusion profiles of cesium and chloride were measured using EPMA and other chemical elements in the sample. We computed the diffusion coefficient by analyzing the diffusion profiles with Fick's law and ionic diffusion model in porous solid with surface charge. The following conclusions were drawn:

- The diffusion of chloride is faster than cesium in all samples.
- In contrast to samples without Al-tobermorite, in which chloride concentration was higher all along the diffusion path, in the samples containing Al-tobermorite, the cesium concentration was higher near the diffusion surface.
- Diffusion is slow in the samples with a lower molar ratio of Ca/(Al+Si) in the amorphous C-A-S-H.
- The samples with Al-tobermorite promote diffusion, which a difference in morphology of C-A-S-H might explain.
- Cesium is adsorbed by aggregates that contain a higher amount of alumina. In addition to the chemical composition, the density of the aggregate may play a role in its adsorption behavior.

Acknowledgement

This project was based on a research project collaboration between Nagoya University and Chubu Electric Power Co. Inc., and was partially supported by the “R&D of the safety improvement of nuclear facilities” project by the Ministry of Economy, Trade and Industry of Japan. The authors are grateful to Prof. Tsuneki Ichikawa, Professor Emeritus of Physical Chemistry from Hokkaido University, Japan, and Dr. Kazuo Yamada from National Institute for Environmental Studies, Japan, for the insightful discussions during the preparation of the manuscript.

Author contributions

Abudushalamu Aili: Methodology, Investigation, Validation, Visualization, Writing – original draft. Ippei Maruayam: Project administration, Supervision, Conceptualization, Methodology, Validation, Funding acquisition, Writing – review & editing. Yoshito Umeki: Project administration, Supervision, Conceptualization, Funding acquisition, Writing – review & editing. Kazuhiro Yokokura: Project administration, Supervision, Conceptualization, Funding acquisition, Writing – review & editing.

Funding

The financial support was provided by a research project collaboration between Nagoya University and Chubu Electric Power Co. Inc., and by the “R&D of the safety improvement of nuclear facilities” project by the Ministry of Economy, Trade and Industry of Japan.

Declarations

Conflict of interest: The authors declare no conflict of interest.

References

CSJ: Kagaku Binran Basic Edition II. Maruzen Publishing (2004)

Dauzeres, A., Le Bescop, P., Sardini, P., Cau Dit Coumes, C.: Physico-chemical investigation of clayey/cement-based materials interaction in the context of geological waste disposal: Experimental approach and results. Cem. Concr. Res. 40, 1327–1340 (2010). https://doi.org/10.1016/j.cemconres.2010.03.015

Elakneswaran, Y., Iwasa, A., Nawa, T., Sato, T., Kurumisawa, K.: Ion-cement hydrate interactions govern multi-ionic transport model for cementitious materials. Cem. Concr. Res. 40, 1756–1765 (2010). https://doi.org/10.1016/j.cemconres.2010.08.019

Elakneswaran, Y., Nawa, T., Kurumisawa, K.: Influence of surface charge on ingress of

446 chloride ion in hardened pastes. Mater. Struct. Constr. 42, 83–93 (2009).
447 https://doi.org/10.1617/s11527-008-9368-8

448 Friedmann, H., Amiri, O., Aït-Mokhtar, A.: Physical modeling of the electrical double
449 layer effects on multispecies ions transport in cement-based materials. Cem. Concr.
450 Res. 38, 1394–1400 (2008). https://doi.org/10.1016/j.cemconres.2008.06.003

451 Garboczi, E.J.: Permeability, diffusivity, and microstructural parameters: A critical
452 review. Cem. Concr. Res. 20, 591–601 (1990). https://doi.org/10.1016/0008-
453 8846(90)90101-3

454 Gartner, E., Maruyama, I., Chen, J.: A new model for the CSH phase formed during the
455 hydration of Portland cements. Cem. Concr. Res. 97, 95–106 (2017)

456 Georget, F., Bénier, C., Wilson, W., Scrivener, K.L.: Chloride sorption by C-S-H
457 quantified by SEM-EDX image analysis. Cem. Concr. Res. 152, 1–11 (2022)(a).
458 https://doi.org/10.1016/j.cemconres.2021.106656

459 Georget, F., Wilson, W., Matschei, T.: Long-term extrapolation of chloride ingress : an
460 illustration of the feasibility and pitfalls of the square root law Long-term extrapolation
461 of chloride ingress : an illustration of the feasibility and pitfalls of the square root law
462 Cl - ingress Surface. Cem. Concr. Compos. (2022)(b).
463 https://doi.org/10.13140/RG.2.2.18420.22403

464 Goto, S., Roy, D.M.: Diffusion of ions through hardened cement pastes. Cem. Concr.
465 Res. 11, 751–757 (1981). https://doi.org/10.1016/0008-8846(81)90033-8

466 Gupta, A., Shim, S., Issah, L., McKenzie, C., Stone, H.A.: Diffusion of multiple
467 electrolytes cannot be treated independently: Model predictions with experimental
468 validation. Soft Matter. 15, 9965–9973 (2019). https://doi.org/10.1039/c9sm01780a

469 Hong, S.Y., Glasser, F.P.: Alkali sorption by C-S-H and C-A-S-H gels: Part II. Role of
470 alumina. Cem. Concr. Res. 32, 1101–1111 (2002). https://doi.org/10.1016/S0008-
471 8846(02)00753-6

472 Horiuchi, M., Sugihara, K., Iwasawa, J.: Record of construction of unit 1 Hamaoka
473 nuclear power plant. Concr. J. 13, 11–20 (1975).
474 https://doi.org/10.3151/coj1975.13.8_11

475 Hosokawa, Y., Yamada, K., Johannesson, B., Nilsson, L.O.: Development of a multi-
476 species mass transport model for concrete with account to thermodynamic phase

equilibriums. Mater. Struct. Constr. 44, 1577–1592 (2011). https://doi.org/10.1617/s11527-011-9720-2

Ichikawa, T.: Theory of Ionic Diffusion in Water-saturated Porous Solid with Surface Charge. J. Adv. Concr. Technol. 20, 430–443 (2022). https://doi.org/10.3151/jact.20.430

Ichikawa, T., Yamada, K., Haga, K.: Method for predicting diffusion penetration rate of chloride ions into concrete by EPMA measurement. In: Annual conference of Japan Cement Association. pp. 70–71 (2021)

Johannesson, B., Yamada, K., Nilsson, L.O., Hosokawa, Y.: Multi-species ionic diffusion in concrete with account to interaction between ions in the pore solution and the cement hydrates. Mater. Struct. Constr. 40, 651–665 (2007). https://doi.org/10.1617/s11527-006-9176-y

JSA: Portland cement (JIS R5210). Tokyo, Japanese Stand. Assoc. (1973)

Kari, O.P., Elakneswaran, Y., Nawa, T., Puttonen, J.: A model for a long-term diffusion of multispecies in concrete based on ion-cement-hydrate interaction. J. Mater. Sci. 48, 4243–4259 (2013). https://doi.org/10.1007/s10853-013-7239-3

Lothenbach, B., Nonat, A.: Calcium silicate hydrates: Solid and liquid phase composition. Cem. Concr. Res. 78, 57–70 (2015). https://doi.org/10.1016/j.cemconres.2015.03.019

Maage, M., Helland, S., Ervin, P., Vennesland, Ø., Carlsen, J.E.: Service life prediction of precast concrete structures exposed to chloride environment. Adv. Civ. Eng. 93, (1996). https://doi.org/10.1155/2019/3216328

Martín-Pérez, B., Zibara, H., Hooton, R.D., Thomas, M.D.A.: Study of the effect of chloride binding on service life predictions. Cem. Concr. Res. 30, 1215–1223 (2000). https://doi.org/10.1016/S0008-8846(00)00339-2

Martin, S.I.: Synthesis of tobermorite: A cement phase expected under repository conditions. In: International high-level radioactive waste management conference: progress toward understanding. pp. 1–5. , Las Vegas, NV (United States) (1994)

Maruyama, I., Rymeš, J., Aili, A., Sawada, S., Kontani, O., Ueda, S., Shimamoto, R.: Long-term use of modern Portland cement concrete: The impact of Al-tobermorite formation. Mater. Des. 198, (2021). https://doi.org/10.1016/j.matdes.2020.109297

508 Mori, D., Yamada, K., Hosokawa, Y., Yamamoto, M.: Applications of electron probe
509 microanalyzer for measurement of Cl concentration profile in concrete. J. Adv. Concr.
510 Technol. 4, 369–383 (2006). https://doi.org/10.3151/jact.4.369

511 Page, C.L., Short, N.R., El Tarras, A.: Diffusion of chloride ions in hardened cement
512 pastes. Cem. Concr. Res. 11, 395–406 (1981). https://doi.org/10.1016/0008-
513 8846(81)90111-3

514 Richardson, I.G.: Tobermorite/jennite- and tobermorite/calcium hydroxide-based
515 models for the structure of {C-S-H}: applicability to hardened pastes of tricalcium
516 silicate, $β$-dicalcium silicate, Portland cement, and blends of Portland cement with
517 blast-furnace slag, meta. Cem. Concr. Res. 34, 1733–1777 (2004).
518 https://doi.org/https://doi.org/10.1016/j.cemconres.2004.05.034

519 Richardson, I.G.: Model structures for C-(A)-S-H(I). Acta Crystallogr. Sect. B Struct. Sci.
520 Cryst. Eng. Mater. 70, 903–923 (2014). https://doi.org/10.1107/S2052520614021982

521 Rymeš, J., Maruyama, I., Shimamoto, R., Tachibana, A., Tanaka, Y., Sawada, S.,
522 Ichikawa, Y., Kontani, O.: Long-term material properties of a thick concrete wall
523 exposed to ordinary environmental conditions in a nuclear reactor building: The
524 contribution of cement hydrates and feldspar interaction, (2019)

525 Samson, E., Marchand, J.: Modeling the effect of temperature on ionic transport in
526 cementitious materials. Cem. Concr. Res. 37, 455–468 (2007).
527 https://doi.org/10.1016/j.cemconres.2006.11.008

528 Samson, E., Marchand, J., Beaudoin, J.J.: Modeling the influence of chemical reactions
529 on the mechanisms of ionic transport in porous materials. An overview. Cem. Concr.
530 Res. 30, 1895–1902 (2000). https://doi.org/10.1016/S0008-8846(00)00458-0

531 Shi, Z., Geiker, M.R., Lothenbach, B., De Weerdt, K., Garzón, S.F., Enemark-
532 Rasmussen, K., Skibsted, J.: Friedel's salt profiles from thermogravimetric analysis and
533 thermodynamic modelling of Portland cement-based mortars exposed to sodium
534 chloride solution. Cem. Concr. Compos. 78, 73–83 (2017).
535 https://doi.org/10.1016/j.cemconcomp.2017.01.002

536 Sui, S., Georget, F., Maraghechi, H., Sun, W., Scrivener, K.: Towards a generic
537 approach to durability: Factors affecting chloride transport in binary and ternary
538 cementitious materials. Cem. Concr. Res. 124, 105783 (2019).
539 https://doi.org/10.1016/j.cemconres.2019.105783

Thomas, M.D.A., Bamforth, P.B.: Modelling chloride diffusion in concrete effect of fly ash and slag. Cem. Concr. Res. 29, 487–495 (1999). https://doi.org/10.1016/S0008-8846(98)00192-6

Tomita, S., Haga, K., Hosokawa, Y., Yamada, K., Igarashi, G., Maruyama, I.: Modeling of the adsorption behavior of cs and sr on calcium silicate hydrates. J. Adv. Concr. Technol. 19, 1061–1074 (2021). https://doi.org/10.3151/jact.19.1061

Xi, Y., Bazant, Z.: Modeling chloride penetration in saturated concrete. J. Mater. Civ. Eng. 11, 58–65 (1999)